Resilient Microgrid Scheduling with Synthetic Inertia from Electric Vehicles within a Network of Charging Stations

Yixun Wen, Zhongda Chu, Amber Srivastava, Fei Teng, and Boli Chen

***Abstract*—Vehicle-to-Grid technologies are proposed as potential providers of virtual inertia for microgrids (MGs). This paper addresses an energy and charging scheduling problem for a MG and investigates how to utilize a network of electric vehicle (EV) charging stations (CSs) to provide sufficient virtual initial for frequency regulation that guarantees the safe transition of MG to the islanded operation during extreme events. The charging behavior of EV within a CS network is complex and can be actively influenced by charge point power and tariff set up by the CS network operator subject to MG operation requirements. A novel modeling framework is proposed to capture these aspects and integrate them into the MG energy management. The goal is to determine the optimal power allocation among distributed energy resources within an MG, minimizing operation costs while ensuring sufficient frequency support with virtual inertia contribution from EVs. To deal with inevitable uncertainties associated with EV arrivals at a CS, we employ joint distributionally robust chance constraints (DRCCs) to mitigate the impact of uncertainty and enhance the robustness of the algorithm. These joint DRCCs are decomposed into individual ones via an optimized Bonferroni approximation method, then suitably relaxed into convex forms, which maintains the solvability of the overall problem. The effectiveness of the method is validated with case studies based on a modified IEEE 14-bus system.**

***Index Terms*—Microgrid Scheduling, Virtual Inertia, Vehicle-to-Grid, Joint Distributionally Robust Optimization**

NOMENCLATURE

Acronyms

BoA	Bonferroni approximation
CG	Conventional Generator
CS	Charging station
DRCC	Distributionally robust chance constraint
EV	Electric vehicle
FR	Frequency response
MG	Microgrid
OCGT	Open Cycle Gas Turbine
PV	Photovoltaic
RES	Renewable Energy Resource
SI	Synthetic inertia
SoC	State of charge
WT	Wind turbines

Indices and Sets

$\mathcal{V}$	Set of all CSs in the MG
$\boldsymbol{G}/g$	Set and indices of CGs within the MG
$\boldsymbol{K}_i/k$	Set and indices of EV fleets in charging station i
s	Index of MG operation scenarios

Parameters

$-P^{\min}/P^{\max}$	The maximum discharging/charging power output of a single charger
$-P_{PV}^{disc}/P_{PV}^{ch}$	The maximum discharging/charging power output of the PV storage system
$\Delta\dot{f}$	The rate of change of frequency (RoCoF)
Δf_{qss}	Quasi-steady-state frequency deviation
π_s	The probability of scenario s
$\tilde{P}_s^{WT}/\tilde{P}_s^{PV}/\tilde{P}_s^{load}$	The predicted power output of wind turbine/PV/load for scenario s
$\varepsilon^0/\varepsilon^{dep}$	Initial SoC of EV fleets/ expected SoC when leaving
$\varepsilon^{\min}/\varepsilon^{\max}$	The minimum/maximum allowable SoC of EV fleets
$C^{run}/C^{start}/C^M$	Financial cost of running CGs/starting CGs/trading with the main grid
D	Damping of the system
$E^{arr}(t)$	The energy of arrival EVs
$N^{arr}(t)$	The number of arrival EVs
N_f	The total number of EV fleets
T	the optimization time horizon
Z^{EV}	The capacity of a single EV

Variables

$\Delta P_{EV,t}$	The additional power provided by EVs for frequency support at time t
$\mathbf{E}(t)$	Energy state vector of EV fleets
$\mathbf{E}^{dep}(t)$	Energy state vector of departure EVs
$\mathbf{L}^{EV}(t)$	EV number vector of departure EVs
$\mathbf{N}^{EV}(t)$	EV number vector of EV fleets
$\mathbf{P}_{EV}(t)$	Charging or discharging power vector of EV fleets
$\bar{\varepsilon}_k(t)$	The average SoC of the kth EV fleet at time t
$H/H^{CG}/H^{EV}$	Inertia of the system/of all CGs in the MG/ synthetic inertia form EVs
$Q(t)$	The number of EVs in the queue

This work was supported in part by the UCL/IITD Strategic Partner Fund (MRP 444), in part by the UCL Research Progression Award, and in part by the EPSRC under Grant EP/Y025946/1.

Y. Wen and B. Chen are with the Department of Electronic and Electrical Engineering, University College London, UK, WC1E 6BT (yixun.wen.22@ucl.ac.uk; boli.chen@ucl.ac.uk).

Z. Chu and F. Teng are with the Department of Electrical and Electronic Engineering, Imperial College London, UK, SW7 2AZ (z.chu18@imperial.ac.uk; f.teng@imperial.ac.uk).

Amber Srivastava is with the Department of Mechanical Engineering, IIT-Delhi, India (asrvstv@iitd.ac.in).

I. INTRODUCTION

Power grids are one of the most critical systems that require significant transformation with the goal of reducing carbon emissions and enhancing energy efficiency [1]. The potential

of renewable energy resources has been explored [2], leading to the widespread implementation of renewable generators and the adoption of clean energy-dependent loads, such as electric vehicles (EVs). The growing penetration of distributed generators, energy storage systems and flexible loads [3] allows forming microgrids (MGs) to coordinate different resources and enable localized optimal energy management [4]. Moreover, MGs are able to enhance the resilience of energy supply by isolating from the main grid and operating in islanded mode during extreme events [5]. However, due to the sudden loss of power and frequency support from the main grid during the transition, the MG may experience power imbalances and frequency instability. This makes MG scheduling of distributed energy resources even more crucial to maintain frequency stability [6]–[8], which will be the focus of the present paper.

With a high penetration of renewable energies, the system inertia significantly decreases due to the reduced presence of conventional synchronous generators [9], leading to faster and more vulnerable frequency dynamics. To compensate for low-inertia power systems, many studies have been focusing on the frequency stability of the main grid or the islanded MG. In [10], frequency constraints are incorporated into the unit commitment problem of the main grid for the first time. Frequency supports from wind turbines (WT) and photovoltaics (PVs) for isolated MGs are proposed in [11], [12], addressing both the low-level control phase and the high-level planning phase. However, only a few studies focus on the frequency dynamics of the MG during the transient period when the MG switches from connected mode to islanded mode. Frequency dynamics during the transient period including synthetic inertia (SI) provision from WTs are considered, and corresponding frequency constraints are reformulated and incorporated into the MG scheduling problem. Frequency dynamics including SI provision from WTs, and PVs are considered in [13], [14], to guarantee the frequency constraints during MG islanding events. However, relying on renewable energy sources for frequency support is often uneconomical due to the need to maintain headroom during normal operation. Hence, it is of great interest to investigate other frequency regulation agents like battery storage systems and EVs, which are capable of immediate bidirectional power transfer during the transition process.

Frequency support from EVs for low inertia system is investigated in [15]–[17]. However, onsite EV numbers are formulated in the scheduling problem as a given external input (based on historical data) rather than a decision variable that can be optimised. Additionally, the use of EVs to support MG islanding transitions is not explored in the aforementioned works. In cases of sudden power imbalance resulting from an islanding event, frequency support must react in a short-term transient period to mitigate frequency deviations [18]. The amount of frequency support from EVs is limited by the number of EVs that are plugged-in inside the MG. This highlights the need for better planning, especially for charging stations (CSs), which involve complex interactions with EVs. EV owners or charging navigation systems [19], [20] select CSs based on factors such as charge point power, expected vehicle dwell times, traffic, CS locations, and tariffs. Some of these factors can be directly or indirectly influenced by grid operations, promoting an integrated coordination scheme rather than siloed, sequential decision-making. Despite the rich literature in scheduling for charging networks that also takes both power grid and transportation into account [21]–[23], the study on the contribution of CS network to the frequency support of the MG remains obscure.

On the other hand, to tackle the uncertainties involved in MG scheduling problem (e.g., load, wind, solar), chance constraints are frequently used in MG scheduling to restrict the violation risk of constraints within an acceptable rate. Specifically, distributionally robust chance constraints (DRCCs) have great advantages over other chance constraints in that the full probabilistic distribution of uncertainties is not required [24], and they are widely applied in grid scheduling problems. In [13], uncertain noncritical load shedding is modeled in a DRCC form to ensure a resilient MG scheduling. In [25], deep learning methods are used to construct the ambiguity set representing WT output power while the DRCC is applied to deal with WT uncertainties in economic dispatch optimization. In [26], a data-driven DRCC method is proposed to tackle multiple uncertainties, including virtual inertia uncertainty and wind power uncertainty for the scheduling problem. To provide enhanced guarantees regarding the overall system stability [27], uncertainty-involved constraints need to be formulated into a joint form, allowing for the simultaneous fulfillment of multiple constraints while maintaining an acceptable joint violation rate [28]. However, obtaining tractable solutions for the joint DRCC is challenging, as exact reformulations are often elusive. Therefore, various approximation methods for joint DRCCs, such as Bonferroni approximation (BoA) are commonly utilized in many works [29], [30]. The main challenge of the BoA is in allocating the violation probability among individual chance constraints. A common approach is to separate the joint violation probability equally among individual chance constraints. However, this usually leads to overly conservative estimates.

This article aims to fill the aforementioned research gaps by a novel resilient MG scheduling paradigm, which can explicitly fuse the complex behavior of EVs among a network of CSs in MG scheduling for enhanced resiliency. The results can maintain sufficient overall inertia for the system and can be used as cost-effective references for low-layer control. The main contributions of the paper are summarized as follows:

1) The proposed day-ahead scheduling provides MG operator with a plan that takes into account both MG operation requirements from CS and the costs required for CS to incentivize EVs. To bridge MG operation and on-road EVs for an enhanced energy management solution, a dynamic EV charging behavior model within a CS network is developed, which takes into account queuing, extra dwelling for recharging the grid, and navigation to alternative CSs in case of congestion. Consequently, the SI provision from EVs can be accurately included in the frequency constraints arising from frequency dynamics in the transient islanding period, ensuring adequate inertia for MG islanding events.
2) The joint DRCCs are applied to handle the uncertain

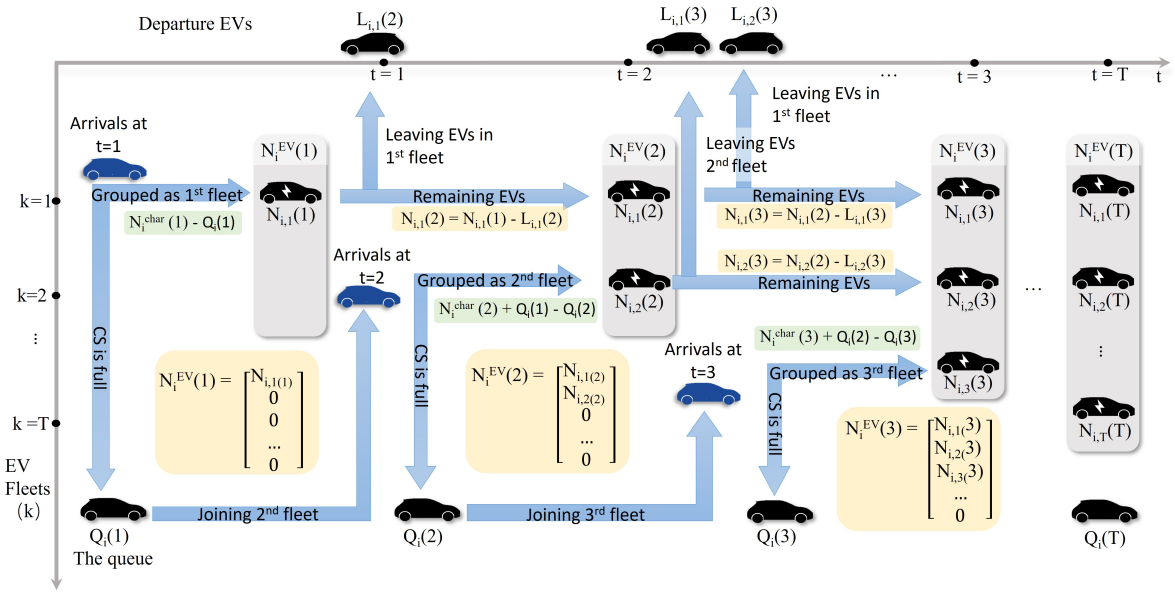

Figure 1. EV flows at the i-th charging station.

error between estimated numbers of arriving EVs and real arriving EVs at CSs and restrict overall violation rates of EV charging/discharging power and SOC level limits in each time slot. In contrast to the classic BoA method, an optimized BoA method is utilized in the paper to separate the joint constraints, which can be less conservative [31]. Additionally, the effect of uncertainties on each time slot is evaluated and optimized by an extra decision variable, which narrows down the impact range of uncertainties and leads to a less conservative solution.

3) The effectiveness of the proposed method is validated with case studies based on a modified IEEE 14-bus system. It is demonstrated that the extended dwelling time of EVs can substantially enhance the SI provision, thereby diminishing the total operational cost of the system. Furthermore, the consideration of EV navigation among a CS network can diminish queueing time, hence alleviating the adverse impact on queuing time resulting from the prolonged presence of EVs.

The rest of the paper is organized as follows: Section II introduced the dynamic model for EV at a single CS and the interaction between CSs. Section III constructs the frequency-constrained day-ahead MG scheduling problem framework with DRCC constraints. Section IV elaborates on case studies and simulation results, and Section V concludes this work.

Notation: Let $\mathbb{R}$, $\mathbb{R}_{\geq 0}$, $\mathbb{R}_{>0}$, $\mathbb{N}$, and $\mathbb{N}_{>0}$ denote the real, the non-negative real, the strict positive real sets of numbers, set of natural numbers, and the set of positive integers, respectively.

II. Dynamic Model for EVs among a CS Network

This section proposes a dynamic system model that captures EV dynamic behaviors within a CS network to enhance EV frequency support ability. From a day-ahead planning perspective, it is reasonable to group certain EVs as a fleet rather than modelling each EV individually. To achieve more precise scheduling of the EV charging/discharging scheme and the associated frequency support provision, both the average state of energy of the EV fleet and the number of EVs involved are modeled.

A. Dynamic Model of EVs at a Single CS

This subsection proposes a system model including both the quantity and average energy level of EVs at a single CS as illustrated in Figure 1. Consider $T_h \in \mathbb{R}_{>0}$ the planning horizon time length and $T \in \mathbb{N}_{>0}$ the number of time steps, and let the time steps for the dynamic system be indicated by $t = 0, 1, \ldots, T$. The arrival of all EVs over the entire period T can be divided into T fleets to model the changes in the number of EVs connected to the charger, while the number of EVs being disconnected from the charging station at each time step serves as the control input. The state of EV numbers in a single CS has the following dynamics:

$$\begin{aligned}\mathbf{N}_i^{EV}(t+1) = \mathbf{N}_i^{EV}(t) - \mathbf{L}_i^{EV}(t+1) \\ +(N_i^{char}(t+1)+Q_i(t)-Q_i(t+1))\cdot \mathbf{e}^{t+1},\ i \in \mathcal{V},\end{aligned} \tag{1}$$

where $\mathbf{N}_i^{EV}(t) = [N_{i,1}(t)\ N_{i,2}\ \cdots\ N_{i,T}(t)]^\top \in \mathbb{N}^T$, $\mathbf{L}_i^{EV}(t) = [L_{i,1}(t)\ L_{i,2}\ \cdots\ L_{i,T}(t)]^\top \in \mathbb{N}^T$ are the number of EVs that are connected to the charger and leaving the CS at time t, respectively. Specifically, the k-th elements $N_{i,k}(t)$ and $L_{i,k}(t)$ denote the number of charging and leaving EVs from the k-th EV fleet at time t. $L_{i,k}(t)$ is modelled as the control variable in (1). The initial condition $\mathbf{N}_i^{EV}(0) = [N_{i,1}(0)\ N_{i,2}(0)\ \cdots\ N_{i,T}(0)]^\top$ follows $N_{i,k}(0) = 0, \forall k > 1$ and $N_{i,1}(0) \geq 0$ denotes the residual vehicles in CS before scheduling. $\mathcal{V} = \{1, 2, \ldots, \iota\}$ is a finite nonempty set of all CSs in the MG, with ι representing total number of CSs within the network, i is the indices of CSs in the MG, $N_i^{char}(t) \in \mathbb{N}$ is the estimated number of EVs arrivals at CS i at the time t (as illustrated in Section II-B). $Q_i(t) \in \mathbb{N}$ is the number

of EVs in the queue at time t, which will be defined later in (3). $\mathbf{e}^{k+1} \in \mathbb{R}^T$ is the unit vector with all zeros and only the $(k+1)$-th element being 1, so as to merge the the newly connected EV into the $(k+1)$-th fleet, as shown in Figure 1. In addition, for the k-th fleet, there is no EV before $t = k$. Hence, $N_{i,k}(t)$ should satisfy $N_{i,k}(t) = 0$, when $0 \leq t < k$. Provided that EVs will not leave without using charging infrastructures, the number of departing EVs must not exceed the number of existing charging EVs from the previous time slot:

$$L_{i,k}(t+1) \leq N_{i,k}(t). \tag{2}$$

The number of EVs waiting in queue is given by:

$$\begin{aligned} Q_i(t) = \max\{&n_i^{EV}(t-1) + N_i^{char}(t) + Q_i(t-1) \\ &- n_i^{dep}(t-1) - \overline{N}_i^{char}, 0\} \end{aligned} \tag{3}$$

where $n_i^{EV}(t) = \sum_{k=1}^{T} N_{i,k}(t)$ and $n_i^{dep}(t) = \sum_{k=1}^{T} L_{i,k}(t)$ denotes the total number of charging (i.e., occupied EV chargers) and departing EVs at time t, respectively. $\overline{N}_i^{char}$ is the maximum capacity of CS i. Herein, we limit the length of the queue for each time slot by:

$$Q_i(t) \leq Q_{i,max}, \tag{4}$$

where $Q_{i,max}$ represents maximum acceptable queue length of CS i. Considering that the MG may have to compensate the CSs for their efforts to encourage EVs to stay connected to the charger, the connection time for all EVs should be minimized, which is calculated as follows:

$$C^{cs} = \sum_{i \in \mathcal{V}} \sum_{t=1}^{T} \sum_{k=1}^{t} N_{i,k}(t) \Delta t, \tag{5}$$

where Δt is the time interval duration of the MG scheduling, for instance $\Delta t = 24/T$ in the context of day-ahead scheduling.

By analogy to the EV quantity model introduced previously, the dynamics of EV fleet average energy state are regulated by:

$$\begin{aligned} \mathbf{E}_i(t+1) = \mathbf{E}_i(t) + \mathbf{P}_i^{EV}(t)\Delta t \\ + E_i^{arr}(t+1) \cdot \mathbf{e}^{t+1} - \mathbf{E}_i^{dep}(t+1),\ i \in \mathcal{V}, \end{aligned} \tag{6}$$

where $\mathbf{E}_i^{EV}(t) = [E_{i,1}(t)\ E_{i,2}\ \cdots\ E_{i,T}(t)]^\top \in \mathbb{R}_{\geq 0}^T$, $\mathbf{P}_i^{EV}(t) = [P_{i,1}(t)\ P_{i,2}(t)\ \cdots\ P_{i,T}(t)]^\top \in \mathbb{R}^T$ are the total energy and collective charging/ discharging power (positive/negative for charging/discharging) of each EV fleet, respectively. Specifically, the k-th elements $E_{i,k}(t)$ and $P_{i,k}(t)$ represent the total energy and the aggregate charging/discharging power of the k-th EV fleet, the control variable of (6). $\mathbf{P}_i^{EV}(t)$ is the combination of two separate control inputs for charging and discharging $\mathbf{P}_i^{EV}(t) = \varrho^d \beta \mathbf{P}_i^{EV,d}(t) + \varrho^c(1-\beta)\mathbf{P}_i^{EV,c}(t)$ where $\varrho^d = 1.05$, $\varrho^c = 0.95$ are the charging/discharging coefficients respectively, and β is a binary variable indicating whether EVs are discharging or not. $\mathbf{E}_i^{dep}(t) \in \mathbb{N}^T$ is the energy taken by EVs that leave at time t. Total initial energy $E_i^{arr}(t)$ corresponds to the number of EVs that connect to chargers at time t so it can be expressed as:

$$E_i^{arr}(t) = [N_i^{char}(t) + Q_i(t-1) - Q_i(t)]\varepsilon_{i,t}^0 Z^{EV}, \tag{7}$$

where $\varepsilon_{i,t}^0$ is the average initial SoC, Z^{EV} is the prescribed average energy capacity of an EV. The energy of the departing EVs $E_i^{dep}(t)$ in terms of the number of departing EVs at time t is given by:

$$\mathbf{E}_i^{dep}(t) = \mathbf{L}_i^{EV}(t)\varepsilon^{dep} Z^{EV}, \tag{8}$$

where ε^{dep} is the expected SoC level that owners expect their EVs to reach before leaving. The collective charging/discharging power of each fleet is bounded by

$$-N_{i,k}(t)P^{\min} \leq P_{i,k}(t) \leq N_{i,k}(t)P^{\max}, \tag{9}$$

with $P^{\min}, P^{\max}$ denoting the charging infrastructure charging/ discharging limits. Finally, to protect EV battery, the average SoC of each fleet should be within a certain range:

$$\varepsilon^{\min} \leq \bar{\varepsilon}_{i,k}(t) \leq \varepsilon^{\max}, \tag{10}$$

where $\varepsilon^{\min}$, $\varepsilon^{\max}$ are the minimum and maximum SoC limits.

B. Interaction Between Charging Stations

CSs within an MG are interconnected via traffic networks. In a CS network, the charging demand of a CS typically depend on the traffic volume passing through the CSs, which can be obtained from historical data. Meanwhile, CS can influence EVs of choosing stations by dynamically adjusting prices to avoid long queues and to allow for a higher concurrent presence of EVs at individual sites, thereby contributing to SI provision. This section proposes a strategy to estimate $N_i^{char}(t)$, the number of EVs arriving at CS i, based on historical traffic data. Specifically, $N_i^{char}(t)$ is obtained by assigning EVs with charging requirements to different CSs based on MG operation and traffic cost, to reflect the influence of CSs on EVs. The assigning process is optimally decided concurrently with the MG scheduling, hence a more resilient energy management plan can be obtained.

To facilitate the mathematical description, we constructed a simplified traffic network consisting of CSs in the MG and traffic roads connecting them as illustrated in Fig 2. Considering the complexity of the traffic network, it is fair to assume that there always exists a path between any two of the CSs. To streamline the formulation, the CS network is modelled by a simple complete undirected weighted graph $\mathcal{G} = (\mathcal{V}, \mathcal{L})$, where $\mathcal{L} \in \mathbb{R}^{\iota \times \iota}$ is the weighted adjacency matrix that satisfies $\mathcal{L}_{i,i} = 0$, $\mathcal{L}_{ij} = l_{i,j}$ for $i, j \in \mathcal{V}$, where $l_{i,j} \in \mathbb{R}_{>0}$ is the length of the path. Note that $l_{i,j}$ is not necessarily equal to $l_{j,i}$, and $\mathcal{G}$ is assumed to be a simple graph so that $l_{i,j}$ is unique (which can be understood as the length of the optimal path in terms of travel time or energy consumption).

The number of vehicles passing by a certain CS can be described as the overall traffic flow along the roadway adjacent to that CS, and only a portion of these vehicles are EV with charging requirements. Therefore, the number of EVs with charging requirements passing through the i-th CS, $N_i^{arr}(t)$, is estimated by

$$N_i^{arr}(t) = \gamma_i^c \gamma_i^e \eta_i^{in}(t), \tag{11}$$

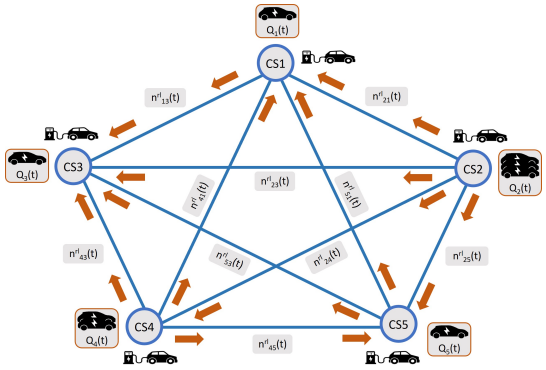

Figure 2. A charging station network connected by roads.

where $\eta_i^{in}(t)$ is the forecasted aggregation of vehicles of roadways traversing CS i, γ_i^e denotes the constant ratio of EVs in the traffic flow, and γ_i^c denotes a split ratio representing the probability of EV to charge up in CS i while on the road. As described in [32], the probability depends on the current SoC of the EV and the minimum acceptable SoC level for not charging. It is expressed using the logistic function as:

$$\gamma_i^c = \left(1 + e^{-\rho(\varepsilon^0 - \underline{\varepsilon})}\right)^{-1} \tag{12}$$

with ρ being a scaling coefficient, and $\underline{\varepsilon}$ being the average EV owners' minimum acceptable SoC levels. Fig. 3 shows the value of γ_i^c against ε^0 when $\rho = 0.15$ and $\underline{\varepsilon} = 30\%$. For

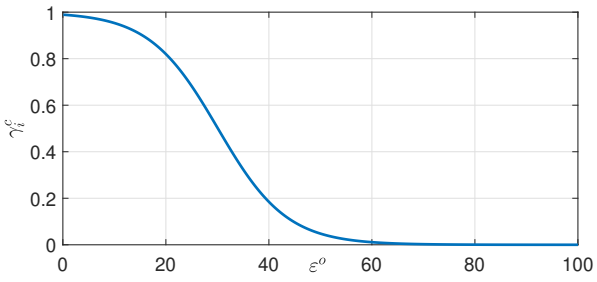

Figure 3. Parameter values of γ_i^c when $\rho = 0.15$, $\underline{\varepsilon} = 30\%$.

$N_i^{arr}(t)$, EVs with charging requirements, CS i is the most convenient CS for EVs along their travel route. However, to enhance the SI provision and alleviate the charging pressure, CSs may guide EVs to other CSs. We model the arriving EVs influenced by CSs as follows:

$$N_i^{char}(t) = N_i^{arr}(t) - \sum_{j\in\mathcal{V}, j\neq i} \xi_{i,j}(t) n_{i,j}^{rl}(t) + \sum_{j\in\mathcal{V}, j\neq i} \xi_{j,i}(t) n_{j,i}^{rl}(t) \tag{13}$$

where $n_{i,j}^{rl}(t)$ is the number of EVs with charging requirements passing through CS i that are guided to CS j within the time slot $[t, t+1)$ or vice versa. Both $n_{i,j}^{rl}(t)$ and $n_{j,i}^{rl}(t)$ are decision variables of the scheduling problem. $\xi_{i,j}(t)$ is a binary variable with $\xi_{i,j}(t) = 1/0$ indicating if there exists EVs being directed from CS i to CS j or not. Note that if EVs passing CS i with charging requirements are directed to CS j within the slot $[t, t+1)$, which means charging at CS j has advantages in time cost or MG operation over CS i within the current time slot, there should be no EVs directed in the opposite direction. Hence $\xi_{i,j}(t)$ satisfy:

$$\xi_{i,j}(t) + \xi_{j,i}(t) = 1. \tag{14}$$

It is important to consider the additional costs incurred by the CS to incentivize electric vehicles to reroute to specific locations. These costs are influenced by the extra time and energy expenditure resulting from the rerouting, which must be factored into the scheduling problem. The traveling time between two CSs is estimated using the latency function as illustrated in [20]. EVs with charging requirements only account for a small fraction of all vehicles on the road, so it is reasonable to assume that their impact on the traffic flow can be ignored. In this context, the traveling time $\Delta t_{i,j}(t)$ required from node i to j can be expressed as:

$$\Delta t_{i,j}(t) = \hat{t}_{i,j} \left[1 + 0.15 \left(\frac{\eta_{i,j}(t)}{\eta_{i,j}^{\max}}\right)^4\right], \tag{15}$$

where $\hat{t}_{i,j} = l_{i,j}/v_{i,j}^{\max}$ is the ideal traffic time with no traffic with $v_{i,j}^{\max}$ being the maximum allowable velocity along the path, $\eta_{i,j}^{\max}$ is the capacity of the path, and $\eta_{i,j}(t)$ is the traffic flow at t. Then the total time cost $C^T(t)$ including traveling and queuing time can be expressed as:

$$C^T(t) = \sum_{i,j\in\mathcal{V}, i\neq j} \xi_{i,j}(t) n_{i,j}^{rl}(x,t) \Delta t_{i,j}(t) + \sum_{i\in\mathcal{V}} \kappa^q Q_i(t), \tag{16}$$

with κ^q denoting a coefficient transforming the number of queuing EVs to the queuing time. Consider the $\overline{v}_{i,j}$ as the average velocity along the path $\{i,j\}$, the energy cost of traveling through this path is evaluated by [33]:

$$\Delta e_{i,j}(t) = \eta_{EV}^{-1} \left(F_r + F_a \overline{v}_{i,j}^2(t)\right) l_{i,j}, \tag{17}$$

where $\Delta e_{i,j}(t)$ is the energy cost, η_{EV} is the energy transition efficiency of EV, F_r is related to the rolling friction of EV, F_a is related to the air resistance. The total energy cost can be expressed as:

$$C^E(t) = \sum_{i,j\in\mathcal{V}, i\neq j} \xi_{i,j}(t) n_{i,j}^{rl}(s,t) \Delta e_{i,j}(t). \tag{18}$$

The total time cost C^{rlc} of the reallocation can be expressed as follows:

$$C^{rlc} = \sum_{t=1}^{T} \left(C^T(t) + \kappa C^E(t)\right), \tag{19}$$

where κ is a coefficient transforming the energy into time cost. Given that the additional energy cost, $C^E(t)$, for rerouting needs to be replenished eventually, the coefficient κ is defined as:

$$\kappa = \frac{1}{P^{\max}} \tag{20}$$

where $P^{\max} = 60$ kW.

III. Distributionally Robust Chance Constrained Day-ahead MG Scheduling Problem

The frequency-constrained day-ahead MG scheduling problem is formulated in this section. To obtain a resilient solution, frequency constraints are derived from frequency dynamics during the transient islanding period and they are incorporated into the MG scheduling problem, and the optimal frequency support provided by conventional generators (CGs) and EVs is decided accordingly. WTs are also capable of providing frequency support, as introduced in [13], [34], but at the cost of stored kinetic energy. To emphasize the effects of frequency support provision from EVs, frequency support from WTs is not considered in this paper. Various uncertainties from WT, PV, loads, and EVs are taken into account to ensure the robustness of the algorithm.

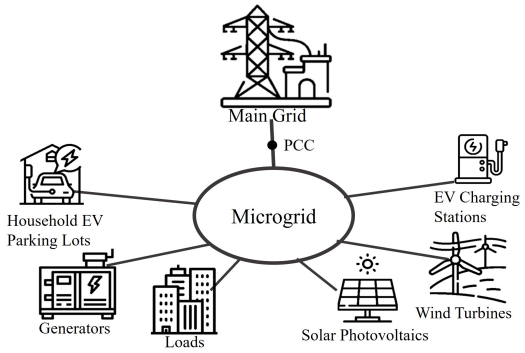

Figure 4. Structure of a microgrid.

As shown in Fig. 4, the MG is comprised of CGs, WTs, PVs, EV CSs, and loads. The power output and on/off states of CGs, the power transaction with the main grid, and the charging/discharging power of EVs are optimally decided subject to the predictions of loads and WT, PV's output power, focusing on minimizing the total cost of MG over the whole time horizon. Uncertainties from WT, PV, and loads are handled by the two-stage stochastic programming, which minimizes the average operation cost for all scenarios. MG's total cost is given below:

$$C^{MG} = \sum_{s\in \boldsymbol{S}} \sum_{t=1}^{T} \pi_s \Big[\sum_{g\in \boldsymbol{G}} \big(C^{run} P^{G}_{g,t,s} \Delta t + C^{start} b_{g,t,s}\big) + C^{M}_{t} P^{M}_{t,s} \Big], \tag{21}$$

where $\boldsymbol{S}$ denotes the set of all potential MG operation scenarios corresponding to diverse weather conditions, with π_s representing the probability associated with each scenario [35]. $\boldsymbol{G}$ denotes the set of all CGs, C^{run} and C^{start} denote the operational and start-up costs of CGs, respectively, $P^{G}_{g,t,s}$ is the power output of CGs, and the binary indicator $b_{g,t,s}$ signifies the operational states of CGs. C^{M}_{t} stands for the electricity trading price while $P^{M}_{t,s}$ is MG's power transaction with the main grid, with positive/negative value indicating the purchase/sale of electricity from/to the main grid. Further constraints of AC power flow and frequency constraints are given below.

A. Power Balance Constraints

The active power balance constraint is as follows:

$$\sum_{g\in \boldsymbol{G}} P^{G}_{g,t,s} + \tilde{P}^{PV}_{s}(t) + \tilde{P}^{WT}_{s}(t) = P^{M}_{t,s} + \tilde{P}^{load}_{s}(t) + \sum_{i\in\mathcal{V}} \sum_{k=1}^{T} P_{i,k,s}(t), \tag{22}$$

with $\tilde{P}^{PV}_{s}(t)$, $\tilde{P}^{WT}_{s}(t)$ denoting predicted output power of PV and WT in scenario s from [35] described by an appropriate scenario tree. $\tilde{P}^{load}_{s}(t)$ is the predicted load of the MG, and $P_{i,k,s}(t)$ represents the value of charging/discharging power $P_{i,k}(t)$ in scenario s. Further conventional AC power flow constraints including the reactive power balance and the line transmission capacity constraints as in [13], are also included for modeling accuracy.

B. Frequency Constraints

The frequency stability of the power system can be evaluated by three indicators: Rate of Change of Frequency (RoCoF), frequency nadir, and steady-state frequency deviation. Frequency constraints are imposed to restrict the three values within the allowable range. The frequency behavior of the power system, enhanced by frequency support from both CGs and EVs, can be described by a swing equation stemming from the concept of Center of Inertia [36]:

$$2H\Delta\dot{f}(t) = -D\Delta f(t) + \Delta R^{CG}(t) - \Delta P_L, \tag{23}$$

with H and D denoting the overall inertia and damping of the system, respectively. ΔR^{CG} is the primary frequency response (FR) from CGs. $\Delta\dot{f}$ represent the value of RoCoF. $\Delta f(t)$ is the frequency deviation. ΔP_L represents the power loss attributed to islanding events, as depicted by a step disturbance. ΔP_L equals the power required from the main grid in this case and is a decision variable. The overall inertia H in (23) can be specifically described as:

$$H = H^{CG} + \sum_{i\in\mathcal{V}} \sum_{k=1}^{T} H^{EV}_{i,k}, \tag{24}$$

where H^{CG} denotes the inertia from CGs. $H^{EV}_{i,k}$ denotes the SI provided by the k-th EV fleet in CS i. Based on the findings of [13], a series of frequency constraints can be derived from (23).

1) RoCoF Constraint: The peak value of RoCoF is achieved at the moment when the islanding event that causes power loss takes place, that is when ΔP_L occurs and FR from CGs haven't responded yet. Hence the constraint of RoCoF can be expressed as:

$$\left| -\frac{\Delta P_L}{2H(t)} \right| \le \Delta \dot{f}^{\max}, \tag{25}$$

with $\Delta \dot{f}^{\max}$ denoting the maximum allowable value of RoCoF.

2) Steady-State Frequency Deviation Constraint: The maximum steady-state frequency deviation is attained as the system returns to the steady state after the occurrence of ΔP_L when $\dot{f} = 0$.

$$\left| \frac{\Delta R^{CG} - \Delta P_L}{D} \right| \leq \Delta f_{qss}^{\max}, \tag{26}$$

with $\Delta f_{qss}^{\max}$ representing the maximum allowable value for the steady-state frequency deviation.

3) Frequency Nadir Constraint: Frequency nadir is assumed to happen when RoCoF reaches 0, hence we can get the time instance when frequency nadir is reached from (23). Then the analytical expression of frequency nadir can be obtained as in [13]. Finally, the frequency nadir constraints are reformulated into the second-order cone form as follows:

$$\left\| \begin{matrix} 2a^2 \\ H - \Delta R^{CG} \end{matrix} \right\|_2 \leq H + \Delta R^{CG}, \tag{27}$$

where $a^2 = \frac{\Delta P_L^2 T_g}{4\Delta f^{\max}} - \frac{\Delta P_L T_g}{4} D$ and $\Delta f^{\max}$ is the maximum allowable value for frequency deviation of nadir.

C. SI Provision from EVs

To better control the RoCoF and frequency nadir within allowable limits, the SI control, which injects additional active power proportional to the RoCoF signal $\Delta \dot{f}$ into the grid, is employed instead of droop control. The corresponding proportionality factor ($H_{i,k}^{EV}$ in (28)) is referred to as SI as it contributes to the value of H (through (24)). SI control from EVs remains inactive as long as the active power balance is maintained. When an event happens causing $\Delta P_L \neq 0$, the energy stored in EV batteries is then utilized to provide additional power for frequency support.

$$\Delta P_{i,k}(t) = -2H_{i,k}^{EV} \Delta \dot{f}, \tag{28}$$

where $\Delta P_{i,k}(t)$ presents the extra SI power provided by the k-th fleet for frequency support. Subsequently, the charging/discharging limits of devices need to be considered as follows when EVs are providing frequency support:

$$-N_{i,k}(t) P^{\min} \leq P_{i,k}(t) - 2H_{i,k}^{EV} \Delta \dot{f} \leq N_{i,k}(t) P^{\max}. \tag{29}$$

As we only consider positive values of H here, we can obtain EV charging/discharging power constraints by combining (9) and (29) as:

$$-N_{i,k}(t) P^{\min} + 2H_{i,k}^{EV} \Delta \dot{f} \leq P_{i,k}(t) \leq N_{i,k}(t) P^{\max}. \tag{30}$$

D. Joint Distributionally Robust Chance Constraints

To address uncertain errors between the real arriving EVs and $N_i^{char}(t)$, constraints (10) and (30) are reformulated into joint DRCC forms in this section. In this way, the overall violation risks of constraints that involve uncertainties derived from arriving EVs are limited to a low rate. The joint DRCCs are then convexified by suitable relaxation, maintaining the solvability of the overall scheduling problem.

First, we define the uncertain errors, $\boldsymbol{\Delta}_i^{arr}$, between the real arriving EVs and $N_i^{char}(t)$ as: $\boldsymbol{\Delta}_i^{arr} = \begin{bmatrix} \delta_{i,1}^{arr} & \delta_{i,2}^{arr} & \cdots & \delta_{i,T}^{arr}, \end{bmatrix}^\top$ in which the element $\delta_{i,k}^{arr}$ represents the error between the actual number of arriving EVs and the estimated arriving EVs at k-th time slot at i-th CS. So for each time slot k, the actual number of arriving EVs, $\tilde{N}_i^{char}(k)$, can be expressed as:

$$\tilde{N}_i^{char}(k) = N_i^{char}(k) + \underbrace{(\mathbf{e}^k)^\top \boldsymbol{\Delta}_i^{arr}}_{\delta_{i,k}^{arr}}. \tag{31}$$

For the k-th EV fleet, $\delta_{i,k}^{arr}$ is introduced to $N_{i,k}(t)$ concurrently with $N_i^{char}(k)$. For the subsequent time slot $t > k$, $\delta_{i,k}^{arr}$ will affect the number of departure EVs, causing deviations in $L_{i,k}(t)$ until the end of the scheduling horizon when all EVs are supposed to leave. We have the following relationship between the deviations of the departure EVs and $\delta_{i,k}^{arr}$.

$$\sum_{t=k+1}^{T} \delta L_{i,k}(t) = (\mathbf{e}^k)^\top \boldsymbol{\Delta}_i^{arr}, \tag{32}$$

where $\delta L_{i,k}(t)$ is the deviations of the number of departure EVs for the k-th EV fleet at time t in CS i. We can then express $\delta L_{i,k}(t)$ as:

$$\delta L_{i,k}(t) = \begin{cases} 0, & t \leq k, \\ \alpha_{i,k}(t)(\mathbf{e}^k)^\top \boldsymbol{\Delta}_i^{arr}, & k < t \leq T, \end{cases} \tag{33}$$

with $\alpha_{i,k}(t)$ representing the portion of uncertain errors $\delta_{i,k}^{arr}$ that affect $L_{i,k}(t)$. We consider $\alpha_{i,k}(t)$ as a decision variable so that the errors can be optimally dealt with. Following (34), $\alpha_{i,k}(t)$ satisfying:

$$\sum_{t=k+1}^{T} \alpha_{i,k}(t) = 1. \tag{34}$$

For $t > k$, the deviation in $N_{i,k}(t)$ caused by uncertain errors will decrease because of the errors handled by $L_{i,k}(t)$, and can be calculated following (33):

$$\delta N_{i,k}(t) = \begin{cases} 0, & t < k, \\ (\mathbf{e}^k)^\top \boldsymbol{\Delta}_i^{arr}, & t = k, \\ h(\alpha_{i,k})(\mathbf{e}^k)^\top \boldsymbol{\Delta}_i^{arr}, & k < t \leq T, \end{cases} \tag{35}$$

where $h(\alpha_{i,k})(t) = 1 - \sum_{\tau=k+1}^{t} \alpha_{i,k}(\tau)$.

The uncertainties in charging numbers of EVs derive from various sources, e.g., uncertain traffic conditions or unpredictable human behaviors. As a consequence, it is difficult to get the full distributional information of the error and commit it to a single distribution pattern. In this case, DRCC is an alternative to original chance constraints which require a specific distribution. DRCC tackles the uncertainty with partial information by limiting the violation rates over a family of probability distributions defined by an ambiguity set (e.g., the moment-based ambiguity sets, distance-based ambiguity sets) that the uncertainty might belong to. Firstly, we define the ambiguity set $\mathcal{P}$ by the first two moments of $\boldsymbol{\Delta}_i^{arr}$ as follows:

$$\begin{aligned} \mathcal{P} = \{ \mathbb{P} : \mathbb{E}_{\mathbb{P}}[\boldsymbol{\Delta}_i^{arr}] = \boldsymbol{\mu}_i^{arr}, \\ \mathbb{E}_{\mathbb{P}}[(\boldsymbol{\Delta}_i^{arr} - \boldsymbol{\mu}_i^{arr})(\boldsymbol{\Delta}_i^{arr} - \boldsymbol{\mu}_i^{arr})^\top] = \boldsymbol{\Sigma}_i \} \end{aligned} \tag{36}$$

with $\boldsymbol{\mu}_i^{arr} = \begin{bmatrix}\mu_{i,1} & \mu_{i,2} & \cdots & \mu_{i,T}\end{bmatrix}^\top$ being the mean and $\boldsymbol{\Sigma}_i$ being the covariance matrix. To guarantee high overall security of the system, we reformulate constraints (10) and (30) into joint DRCC form and substitute (33), (35) as follows:

$$\begin{aligned}\inf_{\mathbb{P}\in\mathcal{P}}\mathbb{P}\Big[&E_{i,k}(t)\le(N_{i,k}(t)+h(\alpha_{i,k}(\mathbf{e}^k)^\top\boldsymbol{\Delta}_i^{arr})E^{\max},\\&(N_{i,k}(t)+h(\alpha_{i,k}(\mathbf{e}^k)^\top\boldsymbol{\Delta}_i^{arr})E^{\min}\le E_{i,k}(t),\\&P_{i,k}(t)-N_{i,k}(t)P^{\max}\le P^{\max}h(\alpha_{i,k})(\mathbf{e}^k)^\top\boldsymbol{\Delta}_i^{arr},\\&-N_{i,k}(t)P^{\min}-P_{i,k}(t)+2H_{i,k}^{EV}\Delta\dot{f}\\&\qquad\le P^{\min}h(\alpha_{i,k})(\mathbf{e}^k)^\top\boldsymbol{\Delta}_i^{arr},\\&\forall k\in\{1,2,...,t\}\Big]\ge 1-\epsilon\end{aligned}\tag{37}$$

where $E^{\max}=\varepsilon^{\max}Z^{EV}, E^{\min}=\varepsilon^{\min}Z^{EV}$, and ϵ is a predefined risk tolerance of the joint DRCC. There are totally $4t$ constraints in (37), and it means that all constraints in (37) of the first fleet to the t-th fleet are required to be satisfied simultaneously with the probability not lower than $1-\epsilon$.

The joint nature of (37) makes it hard to be reformulated directly into solvable form. Therefore, an optimized Bonferroni approximation scheme [31] is utilized to decompose the joint DRCCs into single DRCCs. Single DRCCs are then approximated into a convex form. In consequence, the solvability of the scheduling problem is maintained. Therefore, (37) can be decoupled as follows:

$$\begin{aligned}\inf_{\mathbb{P}\in\mathcal{P}}\mathbb{P}_k\Big[&\delta_{i,k}^{arr}:E_{i,k}(t)\le(N_{i,k}(t)\\&+h(\alpha_{i,k})(\mathbf{e}^k)^\top\boldsymbol{\Delta}_i^{arr}E^{\max}\Big]\ge 1-\epsilon_{i,k,1}(t)\end{aligned}\tag{38}$$

$$\begin{aligned}\inf_{\mathbb{P}\in\mathcal{P}}\mathbb{P}_k\Big[&\delta_{i,k}^{arr}:(N_{i,k}(t)+h(\alpha_{i,k})(\mathbf{e}^k)^\top\boldsymbol{\Delta}_i^{arr}E^{\min}\le E_{i,k}(t)\Big]\\&\ge 1-\epsilon_{i,k,2}(t)\end{aligned}\tag{39}$$

$$\begin{aligned}\inf_{\mathbb{P}_k\in\mathcal{P}_k}\mathbb{P}_k\Big[&\delta_{i,k}^{arr}:P_{i,k}(t)-N_{i,k}(t)P^{\max}\\&\le P^{\max}h(\alpha_{i,k})\delta_{i,k}^{arr}\Big]\ge 1-\epsilon_{i,k,3}(t)\end{aligned}\tag{40}$$

$$\begin{aligned}\inf_{\mathbb{P}_k\in\mathcal{P}_k}\mathbb{P}_k\Big[&\delta_{i,k}^{arr}:-N_{i,k}(t)P^{\min}-P_{i,k}(t)+2H_{i,k}^{EV}\Delta\dot{f}\\&\le P^{\min}h(\alpha_{i,k})(\mathbf{e}^k)^\top\boldsymbol{\Delta}_i^{arr}\Big]\ge 1-\epsilon_{i,k,4}(t)\end{aligned}\tag{41}$$

$$\sum_{p=1}^{4}\sum_{k=1}^{t}\epsilon_{i,k,p}(t)\le\epsilon_j,\tag{42}$$

where $\epsilon_{i,k,p}(t)$ is an optimal variable and $p\in\{1,2,3,4\}$ represents the p-th inequality constraint in (37). As (38-41) can be approximated and reformulated into convex forms in a similar way, we only take (40) as an example to elaborate the reformulation in the following. According to [37], the DRCC constraint (40) can be relaxed by the following probability inequality

$$\begin{aligned}&-P^{\max}h(\alpha_{i,k})\mu_{i,k}^{arr}+\sqrt{\frac{1-\epsilon_{i,k,3}(t)}{\epsilon_{i,k,3}(t)}}\Big|P^{\max}h(\alpha_{i,k})\sigma_{i,k}\Big|\\&\le N_{i,k}(t)P^{\max}-P_{i,k}(t),\quad\forall k\in\{1,2,...,t\},\end{aligned}\tag{43}$$

where $\sigma_{i,k}^2$ is the variance of $\delta_{i,k}^{arr}$. To deal with the nonconvex term $\sqrt{\frac{\epsilon_{i,k,3}(t)}{1-\epsilon_{i,k,3}(t)}}$ and product of decision variables that appear on the left-hand side of (43), we first reformulate (43) as

$$\kappa_{i,k,3}(t)\le\sqrt{\frac{\epsilon_{i,k,3}(t)}{1-\epsilon_{i,k,3}(t)}}\tag{44}$$

$$\begin{aligned}\Big|P^{\max}h(\alpha_{i,k})\sigma_{i,k}\Big|\le\kappa_{i,k,3}(t)\Big[&N_{i,k}(t)P^{\max}-P_{i,k}(t)\\&+P^{\max}h(\alpha_{i,k})\mu_{i,k}^{arr}\Big]\quad,\forall k\in\{1,2,...,t\}\end{aligned}\tag{45}$$

With $\sqrt{\epsilon_{i,k,3}(t)(1+\epsilon_{i,k,3}(t))}$ being an inner approximation of $\sqrt{\frac{\epsilon_{i,k,3}(t)}{1-\epsilon_{i,k,3}(t)}}$ as shown in Fig. 5, the inequality condition

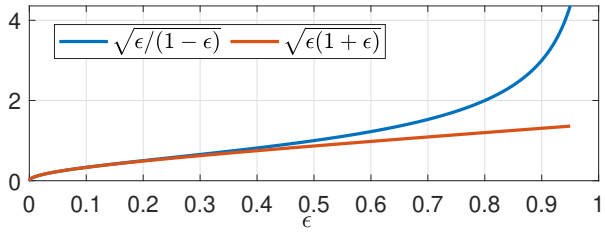

Figure 5. The profiles of $\sqrt{\epsilon/(1-\epsilon)}$ and $\sqrt{\epsilon(1+\epsilon)}$. The maximum deviation is less than 0.5% when $\epsilon_p<0.1$.

(44) can be relaxed into a standard second-order cone form:

$$4\kappa_{i,k,3}^2(t)+1\le(2\epsilon_{i,k,3}(t)+1)^2\tag{46}$$

For (45), we use the binary expansion method to handle the right-hand side term that involves the product of two continuous variables. First, $\kappa_{i,k,3}(t)$ is discretized:

$$\kappa_{i,k,3}(t)=\Delta\kappa\sum_{z=1}^{Z}2^{z-1}u_{i,k,3,z}(t)\tag{47}$$

where $\kappa_{i,k,3}(t)\in[0,\sqrt{\frac{\epsilon}{1-\epsilon}}]$, $\Delta\kappa=\frac{\sqrt{\frac{\epsilon}{1-\epsilon}}}{2^Z}$, $Z\in\mathbb{N}_{>0}$ such that 2^Z is the number of discrete points, and $u_{i,k,3,z}(t)$ is a binary variable. Then the right-hand side of (45) can be modeled as:

$$\|P^{\max}h(\alpha_{i,k})\sigma_{i,k}\|_2\le\Delta\kappa\sum_{i=1}^{Z}2^{i-1}v_{i,k,3,z}(t)\tag{48}$$

$$\begin{aligned}-M(1-u_{i,k,3,z}(t))\le&P^{\max}h(\alpha_{i,k})\mu_{i,k}^{arr}+N_k(t)P^{\max}\\&-P_{i,k}(t)-v_{i,k,3,z}(t)\le M(1-u_{i,k,3,z}(t))\end{aligned}\tag{49}$$

$$-Mu_{i,k,3,z}(t)\le v_{i,k,3,z}(t)\le Mu_{i,k,3,z}(t)\tag{50}$$

with

$$\begin{aligned}v_{i,k,3,z}(t)=u_{i,k,3,z}(t)\Big[&N_k(t)P^{\max}-P_{i,k}(t)\\&+P^{\max}h(\alpha_{i,k})\mu_{i,k}^{arr}\Big].\end{aligned}$$

The big-M method is used in (49) and (50) to model the relation that $v_{i,k,3,z} = [N_k(t)P^{\max} - P_{i,k}(t) + P^{\max}h(\alpha_{i,k})\mu_k^{arr}]$ if $u_{i,k,3,z} = 1$; $v_{i,k,3,z} = 0$ if $u_{i,k,3,z} = 0$.

Combining with other operational and safety constraints, the overall MG scheduling problem can be formulated as a Mixed-Integer Linear Programming (MILP) problem. It can be written as:

$$\min_x C(x) = C^{MG} + \lambda(C^{CS} + C^{rlc}) \tag{51}$$

$$s.t. \begin{cases} Gx = g \\ Hx \le h \\ \|Ax + b\|_2 \le c^\top x + d, \end{cases} \tag{52}$$

where x represents the decision variables $P^G_{g,t,s}$, $b_{g,t,s}$, $P^M_{t,s}$, $\mathbf{P}_{i,k,s}$, $\mathbf{L}^{EV}_i$, H^{EV}, $\alpha_{i,k}$, $\epsilon_{i,k,p}$, $\kappa_{i,k,p}$, $u_{i,k,p,z}$, and $v_{i,k,p,z}$. It subjects to equality constraints $Gx = g$ including (1), (6), (7), (8), (13), (14), (22), and (47); inequality constraints $Hx \le h$ including (2), (4), (25), (26), (42), (48), (49), and (50); second-order-cone constraints $\|Ax+b\|_2 \le c^\top x+d$ including (27) and (46). λ represents a coefficient that can be adjusted according to the willingness of EV owners to participate in MG FR. A smaller value of λ indicates that EV owners are more inclined to sacrifice their time to contribute to MG FR.

IV. Simulation Results

The effectiveness of the proposed MG scheduling method is validated in this section with numerical comparisons with benchmark solutions.

A. Experimental Setup

A modified version of the IEEE 14-bus distribution system is employed in case studies as shown in Fig. 6. A simplified real-world traffic network in Ireland is obtained utilizing hourly traffic data from a case study of Darkwell cloud-hosted data platform [38]. Then EVs' traffic data is obtained by assuming certain EV penetration rate. The optimization problem is solved by Gurobi (10.0.2) in a horizon of 24 hours with the time step being 1 hour, i.e., $T = 24$. The model proposed in [39] and [40] is applied to simulate and calibrate the value of forecast power output from WTs. The predictions of PV output power is obtained from [41]. The weather conditions are obtained from the online numerical forecast of the weather [42]. Then a stochastic unit commitment model in [35] is adopted, where the renewable energy source uncertainties are described by constructing an appropriate scenario tree.

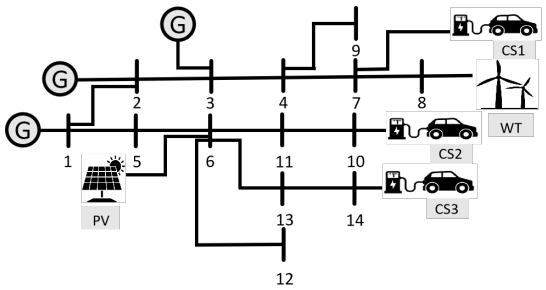

Figure 6. Modified version of IEEE 14-Bus Microgrid System

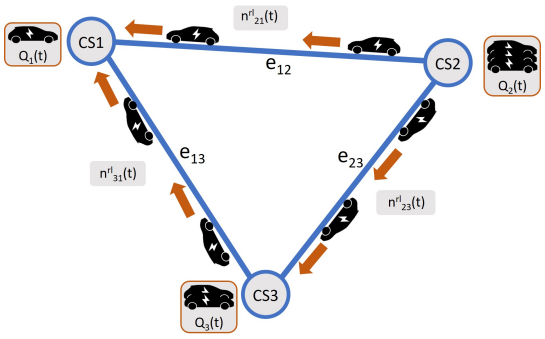

Figure 7. A simple traffic network.

As shown in Fig. 6, PV with the battery storage system is installed on BUS 6, WT is installed on Bus 8, and Open Cycle Gas Turbines (OCGTs) are installed on Bus 1,2 and 3 with a total capacity of 2.50 GW. System Generator parameters and CS parameters are listed in Table I. The simplified traffic

Table I
Simulation Parameters.

Generation	OCGT		
BUS	1	2	3
Number of Unit	20	20	10
Rated Power (GW)	0.05		
No-Load Cost (£/h)	300		
Marginal Cost (k£/GWh)	50		
Startup Cost (£)	600		
Inertia Constant (s)	5		
Max Slow FR Capacity (GW)	0.05		
T_g(s)	10		
System parameters			
System damping D	0.5%		
$\Delta f^{\max}$ (Hz/s)	0.5		
$\Delta f^{\max}$ (Hz)	0.8		
$\Delta f^{\max}_{qss}$ (Hz)	0.5		
CS parameters			
CSs	CS1	CS2	CS3
BUS	7	10	14
Capacity	250	250	250
Max Charge Rate (kW)	60	60	60
Max Discharge Rate (kW)	10	10	10
EV parameters			
Battery capacity (KWh)	100		
F_r (N)	378.28		
F_a (kg)	0.1845		
γ^e_i	60%		
ϱ^d	1.05		
ϱ^c	0.95		

network is shown in Fig 7. The hourly traffic condition data for road connecting CSs is derived from Darkwell cloud-hosted data platform [38] and is shown in Fig. 8. The initial SoCs of EVs upon arriving CSs are modeled as random variables that follow the truncated Gaussian distribution $\varepsilon^0 \in (0.2, 0.6)$ with μ being 30% and σ being 10% as illustrated in [43].

B. Effectiveness Validation of Proposed Model

This simulation demonstrates the effectiveness of the proposed model by comparing the following cases: 1) The baseline case serves as a benchmark that represents common household/parking lot EV charging models utilized in existing

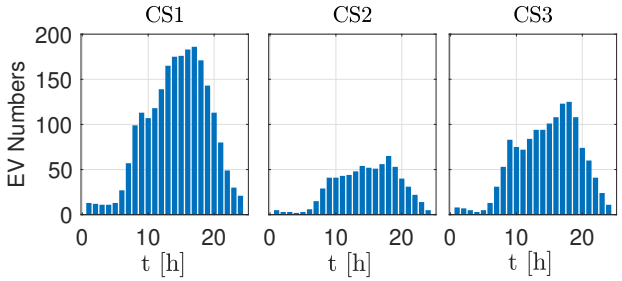

Figure 8. Arriving EVs at the three CSs.

Table II
MG Operational and EV Time Cost.

Cases	Cost(k£)	Total Queuing Time(h)	Traffic Time Cost(h)
Baseline	67.3	814	5154
Case2	63.2	1155	7030
Case3	60.4	548	6495

MG scheduling works [15], [16], where the behaviors of EV follow certain patterns and the number of arriving and departure EVs depend on the historical data, and the influence of CS is omitted. 2) This case only considers the extra dwelling time of EVs in the isolated CS that without EV routing within the charging network. 3) The case proposed in this paper. Total costs of three cases are shown in Table II. Compared with the baseline case, EV extra dwelling time (Case Two) can save up to 6.1% of total cost and further enabling EV routing among the charging network (Case Three) can save 10.4% of total cost. As illustrated in Fig. 9, the SI supplied by EVs is quantified by the value of total H^{EV}. It shows that the SI provided by EVs accounts for more than 85% of the overall system inertia during $t = 8 - 24$ h.

Comparisons of EV numbers across the three cases are depicted in Fig. 10. As illustrated, Case Three significantly contributes to the provision of SI. Specifically, Case Three provides an average of 31% more SI during $3 - 6$ h, 8% during time $13 - 16$ h, and 153% during $21 - 24$ h. The comparison between Case Two and the Baseline Case reveals that additional dwelling behavior results in an increase in queuing time. However, as demonstrated by Case Three, the consideration of routing within the charging network can mitigate queuing time while preserving the contribution of EVS to SI provision.

Fig. 11 shows the MG operational cost of three cases and the number of operating OCGTs can be represented by the

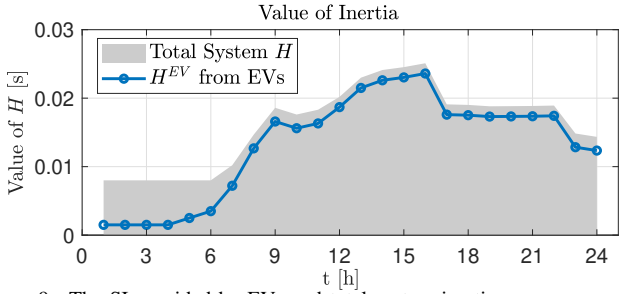

Figure 9. The SI provided by EVs and total system inertia.

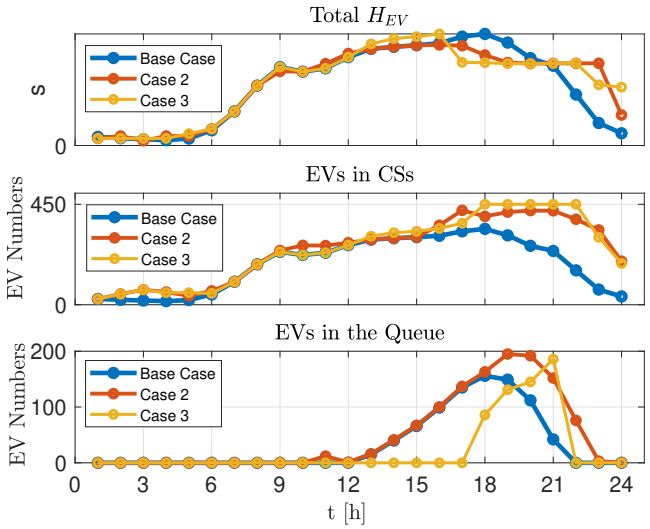

Figure 10. Top: The value of total virtual inertia provided by EVs in three cases. Middle: The total number of EVs connected to the charger in three cases. Bottom: The number of EVs in the queue in three cases.

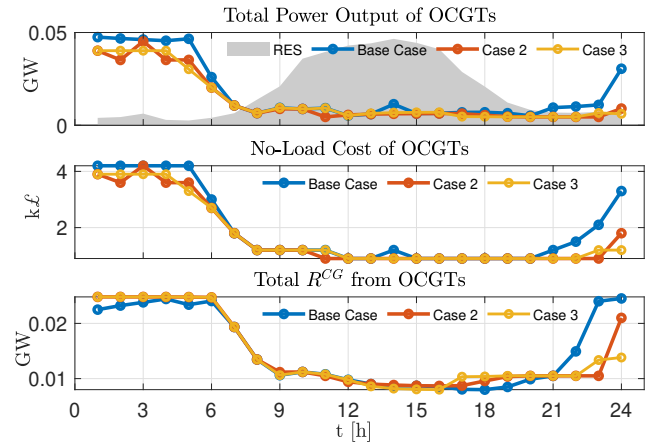

Figure 11. Top: The total power output of OCGTs in three cases and the power output of renewable energy resources (RESs). Middle: The no-load cost in three cases. Bottom: The value of total primary FR provided by OCGTs in three cases.

no-load cost. During the intervals $t = 1 - 7$ h, the power output generated by PVs is constrained and the number of connected EV is limited, which results in a greater reliance on OCGTs for power generation and inertia provision. With a large number of OCGTs in operational states, OCGTs are the main system inertia providers during this period.

During $t = 8 - 18$ h, when the output power of PV is relatively large, only a few OCGTs are in operation, leading to a decrease in system inertia. In the meantime, more EVs have arrived in CSs so CSs are capable of larger SI provision. Consequently, the proportion of SI provided by EVs increases dramatically during this period. Starting from $t = 17$ h, as the output power of PVs declines to a certain level, several OCGTSs are reactivated, leading to a reduction in the total value of H^{EV} derived from EVs. Concurrently, the decreased need for SI provision results in a decrease in the number of connected EV.

It is noteworthy that the no-load cost of Case Two and Three

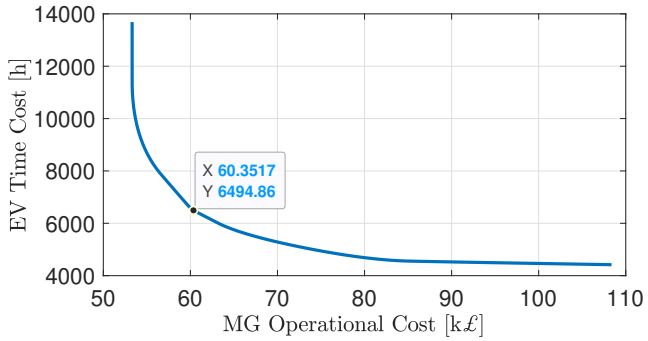

Figure 12. The results of MG operational cost and total time cost with different coefficient λ Values. The horizontal axis represents the MG operation cost, and the vertical axis represents the time cost including dwelling time and relocation time of EVs and the energy cost of relocation that transformed into time cost by κ.

is reduced during $t = 1 - 7$ h and $t = 21 - 24$ h compared to the Baseline Case. On the other hand, more EVs are kept in the CS and more H^{EV} are provided during this period. This proves that the extra dwelling time can contribute to SI provision and decrease the number of operating OCGTs, thus reducing the MG operational cost.

It should be noted that during $t = 16 - 20$ h, although there are more EVs in the CS in Case Two and Three, the quantity of H^{EV} provided is less than the baseline case. This discrepancy arises due to smaller average charging power of EVs caused by the prolonged presence of EVs. During this period, the numbers of operating OCGTs in the three cases are the same. With lower output power, OCGTs have more potential to provide R^{CG}. Hence less SI is required from EVs.

Through the comparison of results across the three cases, it is evident that the additional dwelling time of EVs can significantly contribute to the SI provision, consequently reducing the overall operational cost of the system. Moreover, by considering routing among the charging network, the queuing time can be reduced, mitigating the negative impact of extra dwelling time.

C. Selection of Coefficient λ

Fig. 12 shows the relation between MG operational cost and EV time cost when different values of λ are selected. Specifically, EV time cost includes dwelling time and relocation time of EVs and the energy cost of relocation that transformed into time cost by κ. The value of λ can be adjusted to align with the tendency of EV owners towards providing frequency support or to fulfill the specific requisites of the MG. As illustrated in (51), larger values of λ lead to higher operational costs of MG and less cost for EV incentive, and vice versa. Combined with the result in Table III, it can be found that the MG operational cost increases rapidly when $\lambda > 1e-3$ while the queuing time becomes 0. The queuing time increases largely and even exceeds the Baseline Case when $\lambda < 1e-3$. Hence to minimize the MG operational cost and at the same time maintain acceptable queuing time, $\lambda = 1e-3$ is chosen in our case.

Table III
MG Operational Cost and Total Time Cost with different λ Values.

Value of λ	5e-4	1e-3	4e-3	6e-3
MG Operational Cost	60.0	60.4	80.3	90.3
Total Time Cost	6568	6495	4589	4521
Queuing Time	993	548	0	0

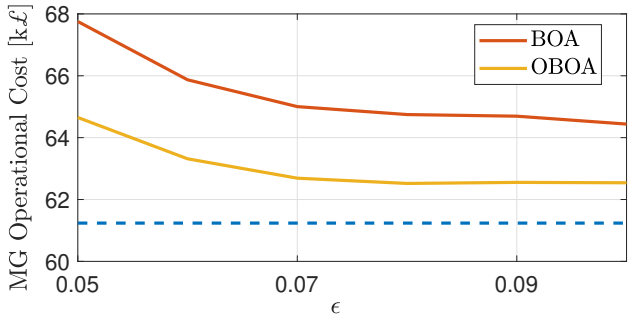

Figure 13. Total cost obtained by different violation rates of the joint DRCC.

D. Effects from Uncertainties

In this section, we examine the impact of incorporating uncertain arriving EVs on MG operations. The mean and variance for arrival EV forecast errors are derived from data in the Darkwell cloud-hosted data platform [38]. Subsequently, various violation rates are applied, and their implications on the operational costs of the MG are evaluated. As illustrated in Fig. 13, we compare the average system costs over a 24-hour period across different cases:

- proposed optimized BoA approximation method to separate joint DRCCs
- classical BoA approximation to separate joint DRCCs
- lower bound solution where violation rates for all individual DRCCs are set to $\epsilon_{i,k,p} = 1$ (no uncertainty case).

As depicted in Fig. 13, the total cost of the extreme case is represented by the blue dotted line. The operational cost of the system exhibits a declining trend with increasing violation risk with a lower bound of the case when $\epsilon_{i,k,p} = 1$. This aligns with expectations, as indicated by (43), a smaller violation rate leads to a larger value of $\sqrt{\frac{1-\epsilon_{i,k,3}(t)}{\epsilon_{i,k,3}(t)}}$. This narrows down the feasible space of decision variables and consequently, leads to an increase in the operational cost of the system.

Notably, the adoption of the optimized BOA approximation leads to a reduction in total costs in contrast to the BOA method, which proves that the optimized BOA method is less conservative than the BOA method. Specifically, when the aggregate violation risk $\epsilon = 0.05$, employing the optimized BOA approximation yields a reduction in total cost by 4.8% compared to the BOA method. However, the cost difference between the two methods diminishes as the violation risk increases. This can be attributed to the fact that the accuracy of the inner approximation employed in (46) degrades as ϵ increases, particularly when $\epsilon > 0.1$, the inner approximation becomes overly conservative.

E. Sensitivity Study of Various $P_{\min}$ Values

In this section, we investigate the impact of different discharging limits of the charger on MG operation. As shown

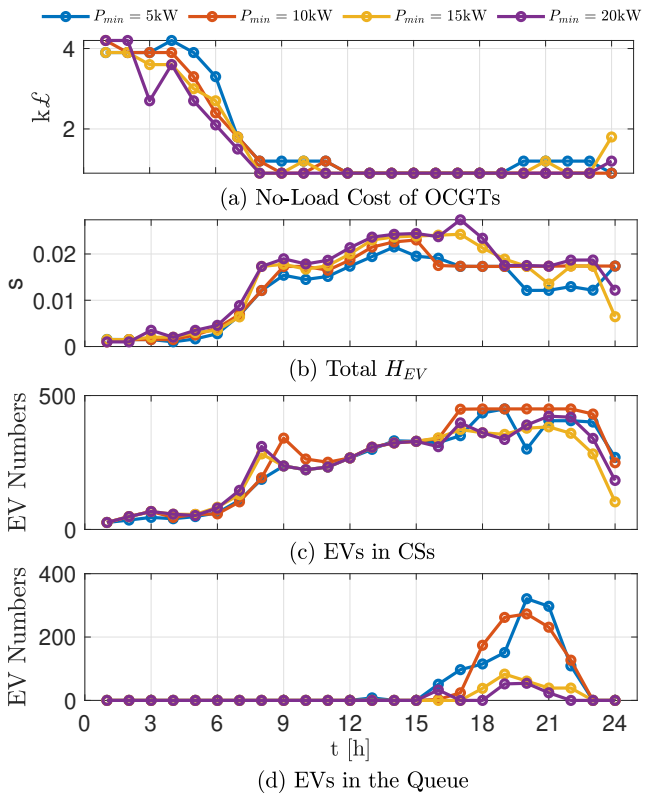

Figure 14. The results of no-load cost, SI provision from EVs, numbers of EVs in CS, and numbers of EVs in the queue with different values of $P_{\min}$.

in Fig. 14(a), the no-load cost of Open Cycle Gas Turbines (OCGTs) decreases as the discharging power limit increases from 5 kW to 20 kW, indicating that EVs contribute more to SI provision. This is further validated in Fig. 14(b), which shows the SI provision from EVs. It should be noted that CS occupation increases as $P_{\min}$ rises from 5 kW to 10 kW, as shown in Fig. 14(c). However, occupation decreases when $P_{\min}$ increases further from 10 kW to 20 kW. This may be because when $P_{\min}$ is limited to 5 kW, the capacity of the CSs can easily become saturated, although more SI provision is requested for optimal operation. With a moderate increase of $P_{\min}$ from 5 kW to 10 kW, the greater SI provision resulting from increased CS occupation leads to more OCGTs being shut down, thus increasing occupation. When $P_{\min}$ further raised to 15 kW and 20 kW, sufficient SI provision can be delivered with even lower CS occupation. During $t = 9-23$ h in these cases, almost no OCGTs are in operation, meaning the onsite EVs can provide sufficient SI, and no additional EVs are needed.

V. Conclusion

This paper presents a microgrid (MG) scheduling problem involving detailed frequency dynamic constraints with electric vehicles (EVs) provision of synthetic inertia (SI). The model of networked charging stations (CSs) are proposed and EV dynamic behaviors including charging/discharging, dwelling, and traveling to neighboring are optimized aiming to fulfill the frequency dynamic requirements during MG islanding period and to minimize the MG operational cost. To guarantee the overall resilience of the system, the uncertain forecast errors from the number of arriving EVs are handled by joint distributionally robust chance constraints (DRCCs). To maintain the solvability of the problem, joint DRCCs are then conservatively separated into individual ones using the optimized Bonferroni approximation method and reformulated into convex forms using reasonable relaxation and linearization. Finally, the effectiveness of the method is validated by case studies based on a modified IEEE 14-bus system. The simulation result shows that the proposed model can save up to 10.4% of the total MG operational cost compared with the baseline case, and SI provided by EVs can account for up to 85% of the total system inertia most of the time.

References

[1] S. Sorrell, "Reducing energy demand: A review of issues, challenges and approaches," *Renewable and Sustainable Energy Reviews*, vol. 47, pp. 74–82, 2015.

[2] O. Ellabban, H. Abu-Rub, and F. Blaabjerg, "Renewable energy resources: Current status, future prospects and their enabling technology," *Renewable and Sustainable Energy Reviews*, vol. 39, pp. 748–764, 2014.

[3] A. Banerji, D. Sen, A. K. Bera, D. Ray, D. Paul, A. Bhakat, and S. K. Biswas, "Microgrid: A review," in *2013 IEEE Global Humanitarian Technology Conference: South Asia Satellite (GHTC-SAS)*, 2013, pp. 27–35.

[4] N. Hatziargyriou, H. Asano, R. Iravani, and C. Marnay, "Microgrids," *IEEE Power and Energy Magazine*, vol. 5, no. 4, pp. 78–94, 2007.

[5] M. Uddin, H. Mo, D. Dong, S. Elsawah, J. Zhu, and J. M. Guerrero, "Microgrids: A review, outstanding issues and future trends," *Energy Strategy Reviews*, vol. 49, p. 101127, 2023.

[6] Z. Fan, B. Fan, and W. Liu, "Distributed control of dc microgrids for optimal coordination of conventional and renewable generators," *IEEE Transactions on Smart Grid*, vol. 12, no. 6, pp. 4607–4615, 2021.

[7] A. Maknouninejad, W. Lin, H. G. Harno, Z. Qu, and M. Simaan, "Cooperative control for self-organizing microgrids and game strategies for optimal dispatch of distributed renewable generations," *Energy Systems*, vol. 3, 03 2012.

[8] K. Mahmud, A. K. Sahoo, J. Ravishankar, and Z. Y. Dong, "Coordinated multilayer control for energy management of grid-connected ac microgrids," *IEEE Transactions on Industry Applications*, vol. 55, no. 6, pp. 7071–7081, 2019.

[9] M. S. Alam, F. S. Al-Ismail, A. Salem, and M. A. Abido, "High-level penetration of renewable energy sources into grid utility: Challenges and solutions," *IEEE Access*, vol. 8, pp. 190 277–190 299, 2020.

[10] L. Badesa, F. Teng, and G. Strbac, "Simultaneous scheduling of multiple frequency services in stochastic unit commitment," *IEEE Transactions on Power Systems*, vol. 34, no. 5, pp. 3858–3868, 2019.

[11] K. V. Vidyanandan and N. Senroy, "Primary frequency regulation by deloaded wind turbines using variable droop," *IEEE Transactions on Power Systems*, vol. 28, no. 2, pp. 837–846, 2013.

[12] H. Xin, Y. Liu, Z. Wang, D. Gan, and T. Yang, "A new frequency regulation strategy for photovoltaic systems without energy storage," *IEEE Transactions on Sustainable Energy*, vol. 4, no. 4, pp. 985–993, 2013.

[13] Z. Chu, N. Zhang, and F. Teng, "Frequency-constrained resilient scheduling of microgrid: A distributionally robust approach," *IEEE Transactions on Smart Grid*, vol. 12, no. 6, pp. 4914–4925, 2021.

[14] Z. Chu, G. Cui, and F. Teng, "Scheduling of software-defined microgrids for optimal frequency regulation," *IEEE Transactions on Sustainable Energy*, 2024.

[15] C. O'Malley, L. Badesa, F. Teng, and G. Strbac, "Frequency response from aggregated v2g chargers with uncertain EV connections," *IEEE Transactions on Power Systems*, vol. 38, no. 4, pp. 3543–3556, 2023.

[16] K. Kaur, N. Kumar, and M. Singh, "Coordinated power control of electric vehicles for grid frequency support: MILP-based hierarchical control design," *IEEE Transactions on Smart Grid*, vol. 10, no. 3, pp. 3364–3373, 2019.

[17] H. Liu, J. Qi, J. Wang, P. Li, C. Li, and H. Wei, "EV dispatch control for supplementary frequency regulation considering the expectation of EV owners," *IEEE Transactions on Smart Grid*, vol. 9, no. 4, pp. 3763–3772, 2018.

[18] Y. Wen, W. Li, G. Huang, and X. Liu, "Frequency dynamics constrained unit commitment with battery energy storage," *IEEE Transactions on Power Systems*, vol. 31, no. 6, pp. 5115–5125, 2016.

[19] T. Qian, C. Shao, X. Wang, and M. Shahidehpour, "Deep reinforcement learning for EV charging navigation by coordinating smart grid and intelligent transportation system," *IEEE Transactions on Smart Grid*, vol. 11, no. 2, pp. 1714–1723, 2020.

[20] X. Shi, Y. Xu, Q. Guo, H. Sun, and W. Gu, "A distributed EV navigation strategy considering the interaction between power system and traffic network," *IEEE Transactions on Smart Grid*, vol. 11, no. 4, pp. 3545–3557, 2020.

[21] Y. Cui, Z. Hu, and X. Duan, "Optimal pricing of public electric vehicle charging stations considering operations of coupled transportation and power systems," *IEEE Transactions on Smart Grid*, vol. 12, no. 4, pp. 3278–3288, 2021.

[22] L. Huang, Y. Jia, X. Han, and P. Wang, "Tri-level dynamic pricing for charging network operator in coupled power-transportation networks," *IEEE Transactions on Smart Grid*, pp. 1–1, 2024.

[23] W. Wei, L. Wu, J. Wang, and S. Mei, "Network equilibrium of coupled transportation and power distribution systems," *IEEE Transactions on Smart Grid*, vol. 9, no. 6, pp. 6764–6779, 2018.

[24] G. Calafiore and L. Ghaoui, "On distributionally robust chance-constrained linear programs," *Journal of Optimization Theory and Applications*, vol. 130, pp. 1–22, 01 2006.

[25] C. Ning and F. You, "Deep learning based distributionally robust joint chance constrained economic dispatch under wind power uncertainty," *IEEE Transactions on Power Systems*, vol. 37, no. 1, pp. 191–203, 2022.

[26] L. Yang, Z. Li, Y. Xu, J. Zhou, and H. Sun, "Frequency constrained scheduling under multiple uncertainties via data-driven distributionally robust chance-constrained approach," *IEEE Transactions on Sustainable Energy*, vol. 14, no. 2, pp. 763–776, 2023.

[27] L. Roald, D. Pozo, A. Papavasiliou, D. Molzahn, J. Kazempour, and A. Conejo, "Power systems optimization under uncertainty: A review of methods and applications," *Electric Power Systems Research*, vol. 214, p. 108725, 01 2023.

[28] L. Yang, Y. Xu, H. Sun, and W. Wu, "Tractable convex approximations for distributionally robust joint chance-constrained optimal power flow under uncertainty," *IEEE Transactions on Power Systems*, vol. 37, no. 3, pp. 1927–1941, 2022.

[29] K. Baker and B. Toomey, "Efficient relaxations for joint chance constrained ac optimal power flow," *Electric Power Systems Research*, vol. 148, pp. 230–236, 2017.

[30] A. M. Hou and L. A. Roald, "Data-driven tuning for chance-constrained optimization: Two steps towards probabilistic performance guarantees," *IEEE Control Systems Letters*, vol. 6, pp. 1400–1405, 2022.

[31] W. Xie, S. Ahmed, and R. Jiang, "Optimized bonferroni approximations of distributionally robust joint chance constraints," *Optimization Online*, vol. 191, 02 2017.

[32] Z. Fotouhi, M. R. Hashemi, H. Narimani, and I. S. Bayram, "A general model for EV drivers' charging behavior," *IEEE Transactions on Vehicular Technology*, vol. 68, no. 8, pp. 7368–7382, 2019.

[33] Y. Wang, J. Jiang, and T. Mu, "Context-aware and energy-driven route optimization for fully electric vehicles via crowdsourcing," *IEEE Transactions on Intelligent Transportation Systems*, vol. 14, no. 3, pp. 1331–1345, 2013.

[34] Z. Chu, U. Markovic, G. Hug, and F. Teng, "Towards optimal system scheduling with synthetic inertia provision from wind turbines," *IEEE Transactions on Power Systems*, vol. 35, no. 5, pp. 4056–4066, 2020.

[35] F. Teng and G. Strbac, "Full stochastic scheduling for low-carbon electricity systems," *IEEE Transactions on Automation Science and Engineering*, vol. 14, no. 2, pp. 461–470, 2017.

[36] A. Gorbunov, J. C.-H. Peng, J. W. Bialek, and P. Vorobev, "Can center-of-inertia model be identified from ambient frequency measurements?" *IEEE Transactions on Power Systems*, vol. 37, no. 3, pp. 2459–2462, 2022.

[37] G. Calafiore and L. Ghaoui, "On distributionally robust chance-constrained linear programs," *Journal of Optimization Theory and Applications*, vol. 130, pp. 1–22, 01 2006.

[38] "Drakewell case study: Transport infrastructure ireland," 2024. [Online]. Available: https://trafficdata.tii.ie/publicmultinodemap.asp

[39] A. Sturt and G. Strbac, "Time series modelling of power output for large-scale wind fleets," *Wind Energy*, vol. 14, no. 8, pp. 953–966, 2011.

[40] ——, "Times-series modelling for the aggregate great britain wind output circa 2030," *IET Renewable Power Generation*, vol. 7, no. 1, pp. 36–44, 2013.

[41] S. Pfenninger and I. Staffell, "Long-term patterns of european pv output using 30 years of validated hourly reanalysis and satellite data," *Energy*, vol. 114, pp. 1251–1265, 2016.

[42] "Met office. weather forecasts," 2024. [Online]. Available: https://www.metoffice.gov.uk/

[43] Z. Wang and R. Paranjape, "An evaluation of electric vehicle penetration under demand response in a multi-agent based simulation," in *2014 IEEE Electrical Power and Energy Conference*, 2014, pp. 220–225.

Yixun Wen received the B.S. degree in electrical engineering from North China Electric Power University, Beijing, China, in 2019 and the M.Sc. degree in electrical and computer engineering from the Georgia Institute of Technology, Atlanta, US, in 2021. She is currently working toward the Ph.D. degree with the Department of Electronic and Electrical Engineering at University College London (UCL), UK. Her research interests include robust optimization and game theory with applications in coupled traffic network and power grid.

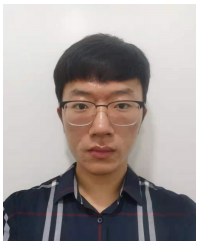

Zhongda Chu (S'18-M'22) received the M.Sc. degree in electrical engineering and information technology from the Swiss Federal Institute of Technology, Zürich, Switzerland, in 2018 and the Ph.D. degree in electrical engineering from Imperial College London, London, U.K., in 2022. He is currently a research associate with the Department of Electrical and Electronic Engineering, Imperial College London. His research interests include control and optimization of power systems with high power electronics penetration.

Amber Srivastava received his B.Tech degree in Mechanical Engineering from the Indian Institute of Technology, Kanpur, in 2014 after which he held employment with an FMCG in India for an year (2014-2015) as an Assistant Manager. Thereafter, he obtained his Masters in Mathematics (2020), and PhD in Mechanical Engineering (2021) from University of Illinois at Urbana Champaign (UIUC), USA. He was a Postdoctoral scholar at the Automatic Control Laboratory, ETH Zürich till 2023. Currently, he is an Assistant Professor at the Indian Institute of Technology Delhi. His broad areas of interest are optimization, learning and controls with applications to network science.

Fei Teng (M'15–SM'21) received the BEng in Electrical Engineering from Beihang University, China, in 2009, and the MSc and PhD degrees in Electrical Engineering from Imperial College London, U.K., in 2010 and 2015. Currently, he is a Senior Lecturer in the Department of Electrical and Electronic Engineering, Imperial College London, U.K. His research focuses on cyber-physical modeling, optimization and data analytics of power systems.

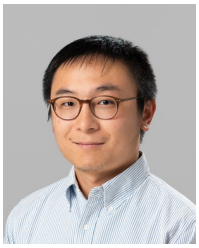

Boli Chen (M'16 - SM'24) received his B.Eng. in Electrical and Electronic Engineering from Northumbria University, UK, in 2010. He earned his MSc and PhD in Control Systems from Imperial College London, UK, in 2011 and 2015, respectively. He is currently a Lecturer in the Department of Electronic and Electrical Engineering at University College London, UK. His research focuses on the control, optimization, and estimation of complex dynamical systems, with rich applications in smart cities, e.g., transportation, electric energy systems, and sensor networks. He serves as an Associate Editor for the IEEE Transactions on Intelligent Transportation Systems and the European Journal of Control. Additionally, he is a member of the EUCA Conference Editorial Board.